Experimental Separation of Sub-Cycle Ionization Bursts in Strong-Field Double Ionization of H_2

Supplemental Material

Václav Hanus, Sarayoo Kangaparambil, Seyedreza Larimian, Martin Dorner-Kirchner, Xinhua Xie, Markus S. Schöffler, Gerhard G. Paulus, Andrius Baltuška, André Staudte, Markus Kitzler-Zeiler

1 Simulations

1.1 Ionization dynamics and sub-cycle bursts

To simulate the ionization dynamics and electron momentum distributions shown in, e.g., Fig. 3 in the main manuscript, we calculate the double ionization and nuclear dynamics using (semi-)classical models for a laser electric field of the form

$$\mathbf{E}(t) = \mathbf{E}_{\parallel} \cos(\omega t + \mathrm{CEP}) + \mathbf{E}_{\perp} \sin(\omega t + \mathrm{CEP}), \tag{1}$$

where $\mathbf{E}_{\parallel}$ and $\mathbf{E}_{\perp} = \varepsilon \mathbf{E}_{\parallel}$ denote the peak electric field strengths along the major respectively minor axis of the polarization ellipse, ε is the ellipticity, and CEP denotes the carrier-envelope phase. Because in our experiments the width of the supersonic gas jet along the laser propagation direction (perpendicular to the $\parallel$ and $\perp$ directions) was cut by adjustable razor blades to about 20 μm, much shorter than the Rayleigh length of the laser beam ($\approx$200 μm), we neglected the dependence of the laser electric field along the laser propagation direction.

Ionization is modeled as described in Ref. 1-SM using a modified ADK-type formula. For the first ionization step, taking place at time t_1, the value of the ionization potential is $I_{p,1} = 15.4$ eV.[2-SM] Ionization-depletion[1-SM] is included for the first ionization step. The first ionization step triggers nuclear motion in the cation H_2^+. The nuclear motion is modeled classically as described in Section 1.3. The second ionization step happens Δt after the first ionization step at time $t_2 = t_1 + \Delta t$, when the two nuclei have reached a certain internuclear distance, R. The ionization potential for the second ionization step, $I_{p,2}(R)$, decreases monotonically with R. We use a linear dependence of the ionization potential $I_{p,2}$ on R. The offset and slope of the linear function $I_{p,2}(R)$ are obtained by a best fit of the simulated to the measured distributions of the kinetic energy release (KER) that results upon fragmentation of the doubly charged parent ion, see Fig. **1-SM**(c). The simulated KER distribution is obtained as described in Section 1.3.

With this model we obtain an ionization rate $w_1(t_1)$ for the first ionization step and an ionization rate $w_2(t_2; R(\Delta t))$ for the second ionization step. The double ionization rate for a given value of Δt is therefore given by $W(t_1, \Delta t) = w_1(t_1) w_2(t_2 = t_1 + \Delta t; R(\Delta t))$, where $R(\Delta t)$ is obtained as described in Section 1.3. With this, the sub-cycle ionization bursts leading to double ionization for a certain value of Δt (e.g. $\Delta t = 1T$ or $1.5T$) and specific values of the CEP, shown in Figs. 3 and 4 of the main manuscript, as a function of absolute time t within the pulse envelope are obtained by plotting $W(t = t_1, \Delta t)$ for the first ionization step (denoted by red lines) and $W(t = t_2 = t_1 + \Delta t, \Delta t)$ for the second ionization (denoted by blue lines).

1.2 Electron momentum distributions

The momentum distributions of the two emitted electrons shown in Fig. 3 of the main manuscript for specific values of Δt and the CEP are calculated by integrating the double ionization rate $W(t_1, \Delta t) =$

$w_1(t_1)w_2(t_2 = t_1 + \Delta t; R(\Delta t))$, described in Section 1.1, over t_1 and binning the values of $W(t_1, \Delta t)$ on a grid for the two electrons' momenta $\mathbf{p}_{e1}$ and $\mathbf{p}_{e2}$. The momenta are obtained from the classical formula $\mathbf{p}_{ei} = -\mathbf{A}(t_i),\ i = 1, 2$ with $\mathbf{A}(t) = -\int_{-\infty}^{t} \mathbf{E}(t')dt'$ derived from the laser electric field defined in Equ. (1).

1.3 Nuclear motion

Nuclear motion is modeled by solving Newton's equations on the $1s\sigma_g$ potential energy curve given in Ref. 3-SM. We assume that upon the first ionization step at the instant t_1 the $1s\sigma_g$ curve of H_2^+ is populated at an internuclear distance R given by the equilibrium distance of H_2. We further assume that the potential energy curve is unaffected by the laser electric field and that the nuclear motion is determined purely by the gradient of the $1s\sigma_g$ curve at any given internuclear distance. The second ionization step takes place at an instant $t_2 = t_1 + \Delta t$. At t_2 the repulsive Coulomb curve is populated and the KER (in atomic units) is calculated as $\mathrm{KER} = \frac{1}{R} + E_K$, where E_K denotes the kinetic energy of the protons acquired during their motion prior to the Coulomb explosion. To obtain a KER distribution from our simulations we loop over the times t_1 and $t_2 = t_1 + \Delta t$ and calculate for each combination the double ionization rate $W(t_1, \Delta t)$ (see Section 1.1). By summing up all combinations of t_1 and $t_2 > t_1$ with their respective double ionization probability W we obtain a distribution of KER, shown in Fig. **1-SM**(c) for the laser pulse parameters used in the experiments, in comparison with the measured KER distribution.

2 CEP-dependent asymmetry of photoelectron emission

As shown in Fig. 2 of the main manuscript and described in text corresponding to this figure, the two-electron emission dynamics strongly depends on the CEP. For certain values of the CEP most of the electrons are emitted with $\mathbf{p}_{\mathrm{rec},\perp} < 0$ (or $\mathbf{p}_{\mathrm{rec},\perp} > 0$). This asymmetric CEP-dependent electron emission can be quantified using the dimensionless asymmetry parameter

$$A = \frac{N(\mathbf{p}_{\mathrm{rec},\perp} < 0) - N(\mathbf{p}_{\mathrm{rec},\perp} > 0)}{N}, \tag{2}$$

where $N(\mathbf{p}_{\mathrm{rec},\perp} < 0)$ and $N(\mathbf{p}_{\mathrm{rec},\perp} > 0)$ denote the number of ionization events that resulted in a negative respectively positive recoil momentum along the direction perpendicular to the main axis of the polarization ellipse, $\mathbf{p}_{\mathrm{rec},\perp} = -(\mathbf{p}_{e1,\perp} + \mathbf{p}_{e2,\perp})$, and N the total number of ionization events. The measured asymmetry parameter $A(\mathrm{KER}, \mathrm{CEP})$ as a function of KER and CEP is shown in Fig. **1-SM** in comparison with the simulated asymmetry distribution obtained with the model described in Section 1 for the laser field defined in Equ. (1). For the comparison in Fig. **1-SM** the constant offset value of the CEP of the experimental data, which is inaccessible in the stereo-ATI technique[4-SM, 5-SM] used in our experiments for determining the CEP, was shifted to obtain best agreement with the simulations. This calibration of the CEP-offset was used throughout this document and also the main article.

The dependence of the asymmetry A on CEP for the three specific cases where Δt is 1, 1.5 and 2 laser cycles is described in detail in the main article in the text corresponding to Figs. 2 and 3. There, it is explained that the CEP can determine whether both electrons are emitted symmetrically around the pulse peak, resulting in $A \approx 0$ (point I in Fig. **1-SM**), or whether they are emitted asymmetrically, resulting, e.g., in a pronounced value $A > 0$ (point II in Fig. **1-SM**). What is not visible in the figures in the main article is the dependence of the asymmetry on the KER. Fig. **1-SM** shows that the asymmetry A markedly depends in KER. As can be seen, it is not possible for a given value of the CEP to obtain the same value of A for all values of KER. For different values of KER the CEP needs to be adapted to obtain the same value of A. For example, to move from point II to point III in the asymmetry distribution, the CEP needs to be shifted by about 40° to stay on the same large value of $A > 0$, resulting in the right-tilt of the colored maxima/minima stripes of the asymmetry distribution. The reason for this correlation between CEP and KER in A is the subtle dependence of the electron momenta on the temporal structure of the sub-cycle ionization bursts discussed in the main manuscript in connection with Fig. 3. From this discussion it becomes clear that the bursts' temporal structure depends differently on the CEP for

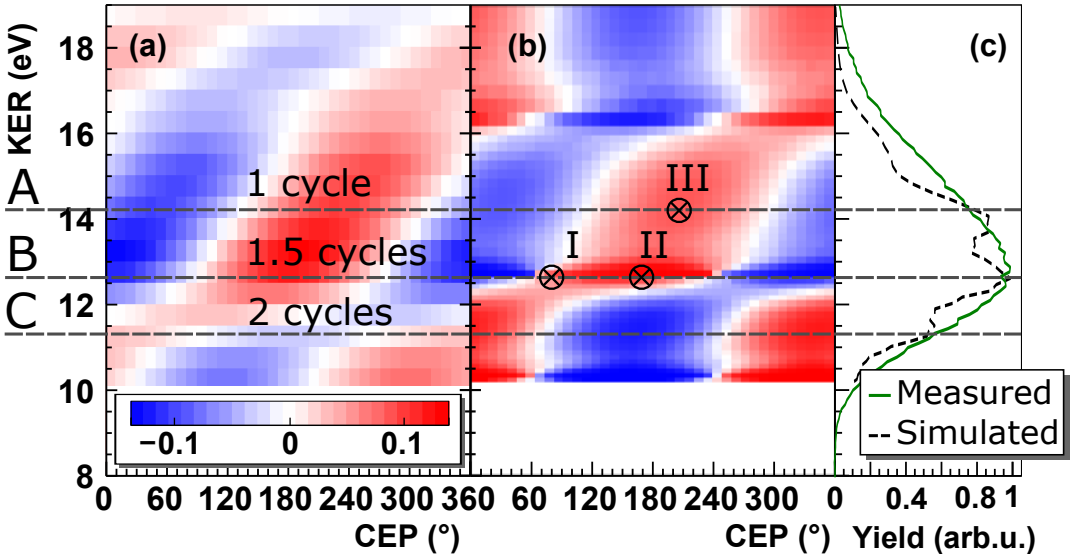

Figure 1-SM: Measured (a) and simulated (b) asymmetry A defined in Equ. (2) as a function of KER and CEP. (c) Measured distribution of KER in comparison with the simulated one obtained as described in Section 1.3. KER values corresponding to an ionization delay of 1, 1.5 and 2 laser cycles, marked by **A,B,C** as in the main article, are indicated. Three specific points in the A-distribution, marked I, II and III are indicated, see text for details.

every value of Δt. Therefore, since Δt is monotonically connected to the value of KER, as explained in Section 1, the CEP is connected in the same way to KER, which explains the correlation between CEP and KER in Fig. 1-SM.

References

1-SM Tong, X. & Lin, C. Time-resolved sequential double ionization of D_{2} molecules in an intense few-cycle laser pulse. *Phys. Rev. A* **70**, 023406 (2004). URL http://link.aps.org/doi/10.1103/PhysRevA.70.023406.

2-SM Dibeler, V. H., Reese, R. M. & Krauss, M. Mass-Spectrometric Study of Photoionization. II. H 2 , HD, and D 2. *J. Chem. Phys.* **42**, 2045–2048 (1965). URL http://aip.scitation.org/doi/10.1063/1.1696245.

3-SM Sharp, T. Potential-energy curves for molecular hydrogen and its ions. *At. Data Nucl. Data Tables* **2**, 119–169 (1970). URL https://linkinghub.elsevier.com/retrieve/pii/S0092640X70800079.

4-SM Rathje, T. *et al.* Review of attosecond resolved measurement and control via carrierenvelope phase tagging with above-threshold ionization. *J. Phys. B At. Mol. Opt. Phys.* **45**, 074003 (2012). URL http://stacks.iop.org/0953-4075/45/i=7/a=074003?key=crossref.159b335739dad85efde2568b4698bb6f.

5-SM Sayler, A. M. *et al.* Precise, real-time, every-single-shot, carrier-envelope phase measurement of ultrashort laser pulses. *Opt. Lett.* **36**, 1 (2011). URL http://www.opticsinfobase.org/abstract.cfm?URI=ol-36-1-1https://www.osapublishing.org/abstract.cfm?URI=ol-36-1-1.